Kink scattering from a parity-time-symmetric defect in the ϕ^4 model

Danial Saadatmand[1],* Sergey V. Dmitriev[2,3],† Denis I. Borisov[4,5],‡
Panayotis G. Kevrekidis[6],§ Minnekhan A. Fatykhov[5],¶ and Kurosh Javidan [1]**
[1]*Department of Physics, Ferdowsi University of Mashhad, 91775-1436 Mashhad, Iran*
[2]*Institute for Metals Superplasticity Problems RAS, Khalturin 39, 450001 Ufa, Russia*
[3]*National Research Tomsk State University, Lenin Prospekt 36, 634050 Tomsk, Russia*
[4]*Institute of Mathematics CC USC RAS, Chernyshevsky 112, 450008 Ufa, Russia*
[5]*Bashkir State Pedagogical University, October Revolution St. 3a, 450000 Ufa, Russia*
[6]*Department of Mathematics and Statistics, University of Massachusetts, Amherst, MA 01003 USA*

arXiv:1411.5857v1 [nlin.PS] 21 Nov 2014

In this paper, we study the ϕ^4 kink scattering from a spatially localized $\mathcal{PT}$-symmetric defect and the effect of the kink's internal mode (IM) is discussed. It is demonstrated that if a kink hits the defect from the gain side, a noticeable IM is excited, while for the kink coming from the opposite direction the mode excitation is much weaker. This asymmetry is a principal finding of the present work. Similar to the case of the sine-Gordon kink studied earlier, it is found that the ϕ^4 kink approaching the defect from the gain side always passes through the defect, while in the opposite case it must have sufficiently large initial velocity, otherwise it is trapped by the loss region. It is found that for the kink with IM the critical velocity is smaller, meaning that the kink bearing IM can pass *more easily* through the loss region. This feature, namely the "increased transparency" of the defect as regards the motion of the kink in the presence of IM is the second key finding of the present work. A two degree of freedom collective variable model offered recently by one of the co-authors is shown to be capable of reproducing both principal findings of the present work. A simpler, analytically tractable single degree of freedom collective variable method is used to calculate analytically the kink phase shift and the kink critical velocity sufficient to pass through the defect. Comparison with the numerical results suggests that the collective variable method is able to predict these parameters with a high accuracy.

PACS numbers: 05.45.Yv, 45.50.Tn

I. INTRODUCTION

About 15 yeas ago the standard notion of Hermiticity in quantum mechanics was challenged by the studies of Bender and co-authors, who demonstrated that a class of non-Hermitian Hamiltonians possess real spectra under the parity-time ($\mathcal{PT}$) symmetry condition, where parity-time means spatial reflection and time reversal, $x \to -x$ and $t \to -t$ [1, 2]. This mathematical discovery has generated an intense interest in the consideration of open physical systems with balanced gain and loss and such systems have been realized experimentally in optics [3–8], electronic circuits [9–11], and mechanical systems [12].

$\mathcal{PT}$-symmetric systems have attracted a great deal of attention from researchers in different branches within physics because they can demonstrate unusual and counterintuitive properties such as unconventional beam refraction [13], Bragg scattering [14], symmetry-breaking transitions [3] and associated ghost states [15–18], a loss-induced optical transparency [4], conical diffraction [19], a new type of Fano resonance [20], chaos [21], non-local boundary effects [22], optical switches [23] and diodes [24, 25], phase sensitivity of light dynamics [26–28], and the possibility of linear and nonlinear wave amplification and filtering [29–31]. 1D and 2D $\mathcal{PT}$-symmetric discrete models can demonstrate unexpected instabilities [32–38]. Extensions of $\mathcal{PT}$-symmetric considerations in the setting of active media with not perfectly balanced gain and loss have also recently been proposed [39–41]. The possibility of a Hamiltonian reformulation of the standard $\mathcal{PT}$-symmetric dimer has been recently demonstrated [42] and calls for the broader question of the potential Hamiltonian/Hermitian nature of such systems in suitable modified variables.

Motivated by the linear oscillator problems associated with the $\mathcal{PT}$-symmetric electrical [9, 10] and mechanical [12] experiments, one of the authors has recently generalized the Klein-Gordon field theory by introducing a $\mathcal{PT}$-symmetric terms within it [43], including the case example of a localized $\mathcal{PT}$-symmetric defect. A collective coordinate method was developed in this work to describe the kink interaction with the defect, see also [44–46]. It was shown that standing kinks in such models are stable if they are centered at the loss side of the defect [45] (and unstable on the gain side), while standing breathers may exist only if centered exactly at the interface between gain and loss regions [46].

It should be pointed out that the interaction of solitary waves with each other [47–50] and with local inhomogeneities of media has been analyzed in various settings. E.g., early works considered the interaction of a fluxon

*Electronic address: saadatmand.d@gmail.com
†Electronic address: dmitriev.sergey.v@gmail.com
‡Electronic address: borisovdi@yandex.ru
§Electronic address: kevrekid@math.umass.edu
¶Electronic address: fatykhovma@mail.ru
**Electronic address: javidan@um.ac.ir

with a non-conservative localized inhomogeneity in a long Josephson junction in [51, 52]. The excitation of both the kink's internal mode (IM) and the defect mode, due to the collision of the kink with a local defect, has been described [53]. The reflection windows were observed in the kink-impurity interactions in the sine-Gordon (SG) [54] and ϕ^4 [55] models. Scattering of the SG breather by localized defects has been investigated [56]. Scattering of linear and nonlinear waves (solitons) on defects in $\mathcal{PT}$-symmetric optical waveguide arrays was analyzed [24, 25, 29–31]. It was shown that the incident high-amplitude solitons (or even linear wavepackets [24, 25]) can excite a mode localized on the $\mathcal{PT}$-symmetric defect. Scattering of wavepackets in such systems was shown to depend on the direction of incidence.

Recently, the interaction of the moving kinks and breathers with the spatially localized $\mathcal{PT}$-symmetric perturbation was investigated in the realm of the SG field [57]. Several new soliton-defect interaction scenarios were observed such as the kink passing/trapping depending on whether the kink comes from the gain or loss side of the impurity, merger of the kink-antikink pair into breather, and splitting of the breather into kink-antikink pair. The collective variable method [43] was successfully applied to calculate the kink phase shift as a result of interaction with the impurity and the threshold kink velocity to pass through the lossy side of the defect.

The SG kink does not support a vibrational IM, while the kinks in the non-integrable ϕ^4 model do support such a mode [58, 59]. It is for that reason that the kink-antikink interactions are far richer in the case of the ϕ^4 model [60, 61]; see also for a recent discussion [62]. When a kink hits an impurity in a conservative model, a part of its energy is trapped towards the excitation of the impurity mode [54, 63] and another fraction leads to the emission of radiation bursts [64]. It is of particular interest to investigate the role of the kink's IM in the case when the kink interacts with the $\mathcal{PT}$-symmetric impurity. This problem is addressed here for the ϕ^4 kinks.

The structure of the paper is as follows. In Sec. II, following the work [43], we introduce the spatially localized $\mathcal{PT}$-symmetric inhomogeneity into the ϕ^4 field and present the well-known ϕ^4 kink solution and the kink's IM profile. In Sec. III, a collective variable method is applied and analytically solved to reveal some features of the kink dynamics in the considered system. We report on the numerical results for scattering of kinks on the $\mathcal{PT}$-symmetric defect in Sec. IV. Our conclusions and some future directions are presented in Sec. V. A number of technical details on the analytical calculations are presented in the Appendix.

II. THE MODEL

We consider the modified ϕ^4 equation of the form [43]

$$a\phi_{tt} - b\phi_{xx} - c\phi(1-\phi^2) = d\gamma(x)\phi_t, \tag{1}$$

where $\phi(x,t)$ is the unknown scalar field, lower indices denote partial differentiation and a, b, c, and d are the coefficients. In terms of new variables $t \to t\sqrt{2a/c}$ and $x \to x\sqrt{2b/c}$, Eq. (1) assumes the dimensionless form

$$\phi_{tt} - \phi_{xx} - 2\phi(1-\phi^2) = \epsilon\gamma(x)\phi_t, \tag{2}$$

in which parameter $\epsilon = \sqrt{2d^2/ac}$ controls the defect amplitude. In order to study the effects of a spatially localized $\mathcal{PT}$-symmetric defect on traveling kinks, for the function $\gamma(x)$ we take

$$\gamma(x) = \tanh(\beta x)\mathrm{sech}(\beta x), \tag{3}$$

which has the symmetry $\gamma(-x) = -\gamma(x)$. Physically this implies that while Eq. (2) describes an open system with gain and loss, the gain balances the loss. Parameter β characterizes the defect inverse width.

For $\gamma(x) \equiv 0$, we have the non-integrable ϕ^4 equation with the following moving kink solution

$$\phi_K(x,t) = \pm\tanh\{\delta_k(x - x_0 - V_k t)\}, \tag{4}$$

where V_k is the kink velocity, x_0 is the kink initial position and $\delta_k = 1/\sqrt{1-V_k^2}$. The energy of the kink is $E_k = 4\delta_k/3$.

An approximate solution (i.e., a solution to leading order in the linearization amplitude A) for the kink bearing IM can be presented in the form [61]

$$\Phi_K(x,t) = \phi_K(x,t) + A\xi(x,t), \tag{5}$$

with the kink's IM mode profile

$$\xi(x,t) = \sqrt{\frac{3}{2}}\tanh\{\delta_k(x-x_0-V_k t)\}\mathrm{sech}\{\delta_k(x-x_0-V_k t)\}. \tag{6}$$

The above Ansatz leads to a kink with the IM having amplitude A and frequency $\omega = \sqrt{3}$. This mode has been discussed by many authors due to its critical role in the collision phenomenology of the ϕ^4 model [60–62]. It should be noted, however, that the above waveform of the so-called "wobbling kink" does not survive indefinitely, but rather decays over time according to a $t^{-1/2}$ law, as discussed, e.g., in [65]; see also references therein.

As it will be shown, the kink's IM noticeably affects the kink dynamics during the interaction with the $\mathcal{PT}$-symmetric defect and it is important from which side the kink hits the defect.

III. COLLECTIVE VARIABLE METHOD

A two-degree of freedom collective variable model, which takes into account not only the kink's translational mode but also the kink's IM has been offered in [43]. The ϕ^4 kink is effectively described by the two degree of freedom particle of mass $M = 4/3$, which is the mass of standing kink. The kink coordinate $\mathcal{X}(t)$ (which in the

unperturbed case is given by $x_0 + V_k t$ as a function of time t) and the kink's internal mode amplitude $A(t)$ can be found from the following equations

$$M\ddot{\mathcal{X}} = \epsilon \int_{-\infty}^{\infty} (\phi'_K + A\xi')[(\phi'_K + A\xi')\dot{\mathcal{X}} - \dot{A}\xi]\gamma(x)dx, \quad (7)$$

$$\ddot{A} = -\omega^2 A + \epsilon \int_{-\infty}^{\infty} \xi[-(\phi'_K + A\xi')\dot{\mathcal{X}} + \dot{A}\xi]\gamma(x)dx. \quad (8)$$

These equations yield the general form of the nonconservative forcing including the coupling between the modes. For the case of weak coupling the above equations simplify as

$$M\ddot{\mathcal{X}} = \epsilon\dot{\mathcal{X}} \int_{-\infty}^{\infty} [\phi'_K(x - \mathcal{X})]^2\gamma(x)dx, \quad (9)$$

$$\ddot{A} = -\omega^2 A + \epsilon \int_{-\infty}^{\infty} [\xi(x - \mathcal{X})]^2\gamma(x)dx. \quad (10)$$

Below in Sec. III A and Sec. III B some analytical results for the simpler single degree of freedom model Eq. (9) are given, while in section IV, we will present the results of numerical solution for the two degree of freedom model of Eqs. (7)-(8).

A. Critical kink velocity

If the kink approaches the defect from the loss side, it must have sufficient momentum in order to avoid trapping. The critical kink initial velocity V_c can be found with the help of the collective variable method. One can present Eq. (9) for $\dot{\mathcal{X}}$ in the form

$$M(\dot{\mathcal{X}} - \dot{\mathcal{X}}_0) = \epsilon\delta_k^2 \int_{-\infty}^{\infty} \int_{\mathcal{X}_0}^{\mathcal{X}} \frac{\gamma(x)dxd\mathcal{X}}{\cosh^4[\delta_k(x - \mathcal{X})]}. \quad (11)$$

A kink having critical velocity must have $\dot{\mathcal{X}} = 0$ at $\mathcal{X} = 0$, i.e., the kink stops when it reaches the center of the defect. Setting in Eq. (11) $V_c = \dot{\mathcal{X}}_0$ and $\dot{\mathcal{X}} = 0$ after integrating over the collective variable $\mathcal{X}$ and x for the initial condition $\mathcal{X}_0$ and recalling that the final stopping point is $\mathcal{X} = 0$ the critical velocity is given by the formula

$$V_c = \frac{32\epsilon\delta_k^2}{M} \left(G_1(1) - \mathrm{e}^{4\delta_k\mathcal{X}_0} G_1(\mathrm{e}^{2\delta_k\mathcal{X}_0})\right). \quad (12)$$

The values of $G_1(1)$ and $G_1(\mathcal{Y})$ can be calculated for the particular cases $\beta = \delta_k$ and $\beta = \delta_k/2$, as it is shown in Appendix VI A. In the former (latter) case the result is given by Eq. (39) (Eq. (40)). For the kink with the initial position $\mathcal{X}_0 \to -\infty$ (far from the defect), one finds $V_c = 32\epsilon\delta_k^2 G_1(1)/M$. For small kink velocity one has $\delta_k \approx 1$ and $M = 4/3$ so that

$$V_c = 0.883\epsilon. \quad (13)$$

The above equation indicates that when a slow kink approaches the loss side of the defect from infinity, its critical velocity V_c is a linear function of the defect amplitude ϵ. Note that this equation was obtained with the help of the collective coordinate method Eq. (9), accounting solely for the center of mass variable without taking into account the kink's IM.

B. Kink's phase shift due to interaction with the defect

The kink approaching the defect from the gain (loss) side is first accelerated (decelerated) and then decelerated (accelerated) when it enters the lossy (gain) side. As a result, the kink experiences a phase shift. The phase shift can be calculated as follows [57]

$$\Delta x = \pm \int_{-\infty}^{+\infty} \frac{\epsilon(F(z) - B)}{\epsilon(F(z) - B) + MV_k} dz, \quad (14)$$

where the plus (minus) shows the case when the kink comes from the loss (gain) side, $V_k > 0$ ($V_k < 0$).

For the kink solution (4) the function $F(z) - B$ can be cast into the particular form

$$F(z) - B = -\delta_k^{-1} \int_z^{+\infty} ds \int_{-\infty}^{+\infty} \frac{\gamma(x)dx}{\cosh^4[\delta_k(x - s)]}. \quad (15)$$

After changing the order of integration and integrating over s one obtains

$$F(z) - B = -\frac{2}{3\delta_k} \int_{-\infty}^{+\infty} \gamma(x) \{1 - \tanh[\delta_k(z - x)] - \frac{\tanh[\delta_k(z - x)]}{2\cosh^2[\delta_k(z - x)]}\} dx. \quad (16)$$

The above integral can be evaluated for the case $\beta = \delta_k$ which is considered below. By evaluating the integral in Eq. (16) and substituting the result into Eq. (14) the kink's phase shift can be found as

$$\Delta x = \pm \frac{1}{\delta_k} G_3\left(-\frac{MV_k\delta_k^4}{\pi\epsilon}\right), \quad (17)$$

$$G_3(\mathcal{Z}) := \int_0^{+\infty} \frac{(y^2 + 4y + 1)dy}{y(y^2 + 4y + 1) - \mathcal{Z}(y + 1)^4}, \quad (18)$$

(see Eq. (41) and Eq. (42) in the Appendix VI B). The phase shift can be calculated only for $\mathcal{Z} \in (-\infty, 0) \cup (3/8, +\infty)$. For $\mathcal{Z} \in (0, 3/8)$ the kink hits the defect from the loss side with the velocity smaller than V_c and is trapped, so that the phase shift diverges. In the Appendix VI B the phase shift is calculated explicitly for the three cases $-\infty < \mathcal{Z} < -1/8$, $-1/8 < \mathcal{Z} < 0$, and $3/8 < \mathcal{Z} < \infty$.

IV. NUMERICAL RESULTS

To study numerically the effect of the $\mathcal{PT}$-symmetric defect on the dynamics of the ϕ^4 kink, we introduce the mesh $x = nh$, where h is the lattice spacing, $n = 0, \pm1, \pm2...$ and propose the following discrete version of Eq. (2)

$$\frac{d^2\phi_n}{dt^2} - \frac{1}{h^2}\left(\phi_{n-1} - 2\phi_n + \phi_{n+1}\right) + \frac{1}{12h^2}\left(\phi_{n-2} - 4\phi_{n-1} + 6\phi_n - 4\phi_{n+1} + \phi_{n+2}\right) - 2\phi_n\left(1 - \phi_n^2\right) - \epsilon\gamma_n\frac{d\phi_n}{dt} = 0, \tag{19}$$

in which $\phi_n(t) = \phi(nh, t)$ and $\gamma_n = \gamma(nh)$. It can be seen that the term ϕ_{xx} in Eq. (2) is discretized with the accuracy $O(h^4)$ which has already been used by other authors [66, 67]. This is done to minimize the effect of discreteness introduced by the mesh.

In order to test the result of the presented analytical method by means of direct numerical simulations we integrated equations of motion (19) with the help of the Störmer method with respect to the temporal variable using an explicit scheme with the accuracy of $O(\tau^4)$ and the time step τ. The simulations were managed for $h = 0.1$ and $\tau = 0.005$.

To solve numerically the collective variable equations of motion Eqs. (7,8), the temporal variable is discretized, $t = j\tau$, where τ is the time step and $j = 0, 1, 2, ...$ The second-order central differences are used to replace $\ddot{\mathcal{X}} \sim (\mathcal{X}_{j-1} - 2\mathcal{X}_j + \mathcal{X}_{j+1})/\tau^2$, $\dot{\mathcal{X}} \sim (\mathcal{X}_{j+1} - \mathcal{X}_{j-1})/2\tau$, and similarly for $\ddot{A}$ and $\dot{A}$. Then Eqs. (7,8) are presented in the form

$$\begin{aligned} a_{11}\mathcal{X}_{j+1} + a_{12}A_{j+1} &= b_1, \\ a_{21}\mathcal{X}_{j+1} + a_{22}A_{j+1} &= b_2, \end{aligned} \tag{20}$$

where

$$\begin{aligned} a_{11} &= \frac{2M}{\tau} - I_1, \quad a_{12} = a_{21} = I_2, \quad a_{22} = \frac{2}{\tau} - I_3, \\ b_1 &= \frac{2M}{\tau}(2\mathcal{X}_j - \mathcal{X}_{j-1}) - I_1\mathcal{X}_{j-1} + I_2A_{j-1}, \\ b_2 &= \frac{2}{\tau}(2A_j - A_{j-1}) - 2\tau\omega^2A_j - I_3A_{j-1} + I_2\mathcal{X}_{j-1}, \\ I_1 &= \int_{-\infty}^{\infty}(\phi_K' + A_j\xi')^2\gamma(x)dx, \\ I_2 &= \int_{-\infty}^{\infty}(\phi_K' + A_j\xi')\xi\gamma(x)dx, \\ I_3 &= \int_{-\infty}^{\infty}\xi^2\gamma(x)dx. \end{aligned} \tag{21}$$

To simulate the kink with initial velocity V_k and initial IM amplitude A, for the initial conditions we set $\mathcal{X}(j = 0) = \mathcal{X}_0$, $\mathcal{X}(j = 1) = \mathcal{X}_0 + V_k\tau$, $A(j = 0) = A(j = 1) = A$.

In the present study the simulations are carried out for different values of the perturbation amplitude ϵ and fixed $\beta = 1$ (the impurity width is approximately equal to the kink width). Since we simulate relatively slow kinks with $\delta_k \approx 1$, the collective variable analytical results, Eqs. (12) and (17,18), calculated for $\beta = \delta_k$ are expected to have a high accuracy.

A. Kinks bearing no initial IM

In Fig. 1 (a) the kink position as a function of time for the kink moving toward the defect from the gain side with the initial velocity $V_k = -0.1$ is presented for the defect amplitudes $\epsilon = 0.1$ and $\epsilon = 0.3$, as indicated for each curve. Solid lines present the result of numerical integration of Eq. (19), while dashed lines give the result of numerical integration of the collective variable model Eq. (9). One can see that the collective variable approach gives a very accurate prediction of the actual kink dynamics. From this figure it is clearly seen that the kink moving toward the defect from the gain side is first accelerated and after passing the gain side of the defect it is decelerated by the loss side. After the kink passes the defect and moves far from it, it seems to restore its initial velocity and energy. The effects of the kink-defect interaction in this case are the phase shift and also the excitation of the kink's internal mode which will be discussed in the following.

Next, suppose a kink comes from the lossy side of the defect. In this case, two different scenarios for the kink interaction with the defect are possible depending on its initial velocity V_k or defect strength ϵ, as presented in Fig. 1 (b) for $\epsilon = 0.1$ and $\epsilon = 0.3$ with $V_k = 0.1$ in both cases. If V_k is large enough or ϵ is small enough, the kink passes through the lossy part of the defect with the velocity smaller than V_k and enters the gain part where it is accelerated up to the initial velocity and then goes on to infinity. In the opposite case (where V_k is not large enough or ϵ is not small enough), the kink does not possess sufficient momentum to pass through the lossy part of the defect and it is trapped there. As one can see from Fig. 1 (b), for the case of $\epsilon = 0.1$, the kink passes through the defect and effectively restores its initial velocity, while for $\epsilon = 0.3$ the kink is trapped by the lossy side of the defect.

In Fig. 1 (c) the kink critical velocity is shown as the function of kink initial position for the two values of defect strength, $\epsilon = 0.1$ and $\epsilon = 0.3$. Numerical results (solid lines) are in a very good agreement with the collective variable results (dashed lines) given by Eq. (12) for the case of $\beta = \delta_k = 1$. The results suggest that for the kink initially located within the loss region of the defect the value of the critical velocity is smaller the smaller ϵ is (which is intuitively clear), as well as smaller the closer one starts to the $x_0 = 0$, i.e., to the center of the $\mathcal{PT}$-symmetric defect.

Fig. 2 shows the kink kinetic energy as a function of

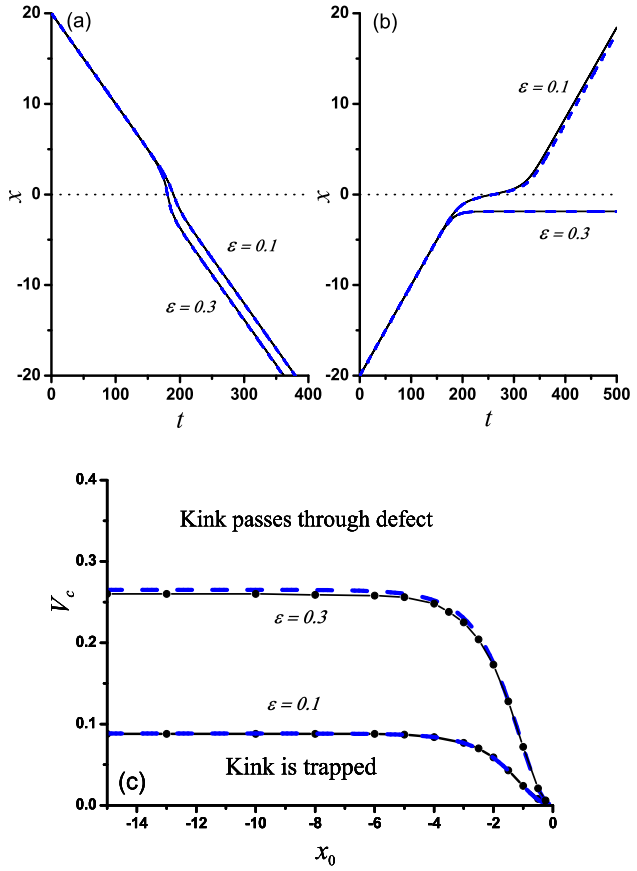

FIG. 1: (Color online) (a,b) Kink position as a function of time for the initial velocity $V_k = \pm 0.1$, for the case when the kink approaches the defect (a) from the gain side, (b) from the loss side. Defect center is located at $x = 0$. (c) Kink critical velocity as a function of its initial position. The results for the perturbation amplitudes $\epsilon = 0.1$ and $\epsilon = 0.3$ are presented. Solid lines show the results of the numerical solution for the continuous system and dash lines show the results obtained with the help of the collective variable method.

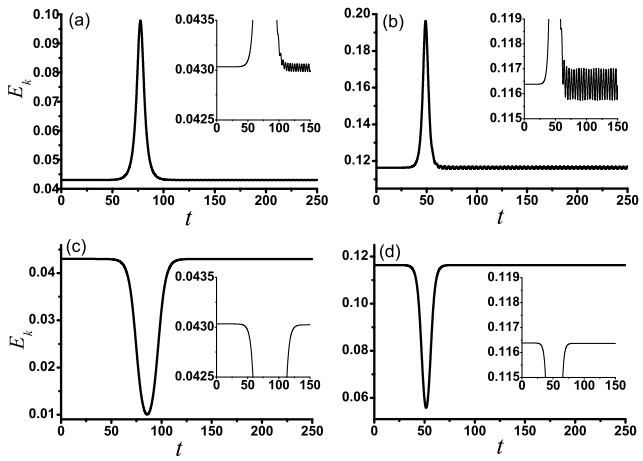

FIG. 2: Numerical results for the continuum model showing the interaction of the kink initially bearing no IM with the $\mathcal{PT}$-symmetric defect of strength $\epsilon = 0.15$. The kink approaches the defect from (a,b) the gain side and (c,d) from the lossy side of the defect. Shown is the kink kinetic energy as a function of time. The kink initial velocity is (a,c) $V_k = 0.25$ and (b,d) $V_k = 0.4$. Different scale used for insets reveals that in (a,b) kink's IM is excited after the interaction with the defect, while in (c,d) it is not excited.

time for the case when the kink, initially bearing no IM, interacts with the $\mathcal{PT}$-symmetric defect with amplitude $\epsilon = 0.15$. In (a,b) the kink approaches the defect from the gain side and in (c,d) from the loss side. The kink initial velocity is $V_k = 0.25$ in (a,c) and $V_k = 0.4$ in (b,d). As a result of interaction with the defect, the kink in (a,b) is firstly accelerated and then decelerated, while in (c,d) it is first decelerated and then accelerated. In both cases the kink's translational velocity after passing through the defect is practically identical to the initial velocity. Note that the kink without the IM excited has a constant in time kinetic energy, while the kinetic energy of the kink with the excited IM oscillates near the constant value with frequency $2\sqrt{3}$, which is double the IM frequency. The insets in (a,b) show that when the kink hits the defect from the gain side, a noticeable IM is excited as a result of the kink-defect interaction, while for the kink coming from the opposite direction [see insets in (c,d)], the IM is much weaker and, in fact, cannot be seen in the scale of the figure. The effect of kink's IM excitation as a result of the interaction with the defect becomes stronger for larger initial kink velocity V_k, as can be seen from comparison of the insets in (a) and (b). However, it is clear that the presence of the IM does not preclude the kink from traveling through the defect, when it comes from the gain side. In fact, as we will see now, quite the opposite is true.

The results obtained for the partial differential equation of (2) and presented in Fig. 2 will be now compared to the results of the numerical solution of Eqs. (7,8) for the two degree of freedom collective variable model, see Fig. 3. In (a,b) we plot the amplitude of the shape mode as the function of time. Here the kink with initial velocity $V_k = \pm 0.4$ hits the defect of amplitude $\epsilon = 0.15$ from the gain side (Fig. 3 (a)) and loss side (Fig. 3 (b)). It can be seen that for the kink coming from the gain side a noticeable IM is excited after the interaction with the defect, whereas for the kink moving in the opposite direction the residual excitation is much weaker and is barely visible in the scale of the figure. This is in very good qualitative agreement with the results for continuum model. In Fig. 3 (c) the amplitude of the shape mode after the interaction with the defect is plotted as the function of kink initial velocity for the case when kink hits the defect from the gain side. The plot (see Fig. 3 (c)) shows that the amplitude increases with increasing kink initial velocity. Again, this is in line with the observations made

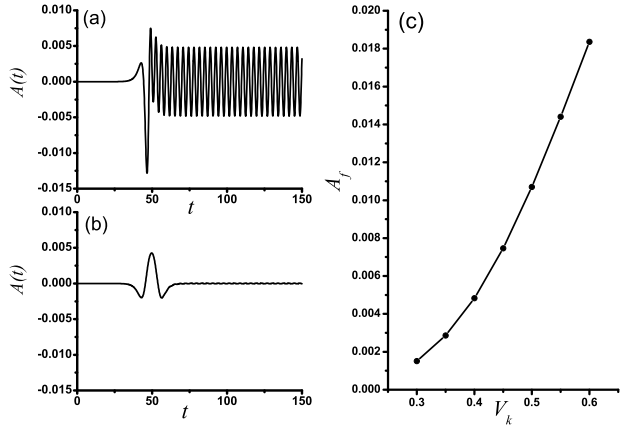

FIG. 3: Collective variable results for the model Eqs. (7,8). (a,b) The dynamics of the internal shape mode whose amplitude $A(t)$ is shown for the case when the kink comes from (a) gain side and (b) loss side. The perturbation amplitude is $\epsilon = 0.15$ and the the initial velocity of the kink is $V_k = \pm 0.4$. (c) Amplitude of the shape mode after the interaction with the defect as a function of kink initial velocity for the case when kink hits the defect from the gain side.

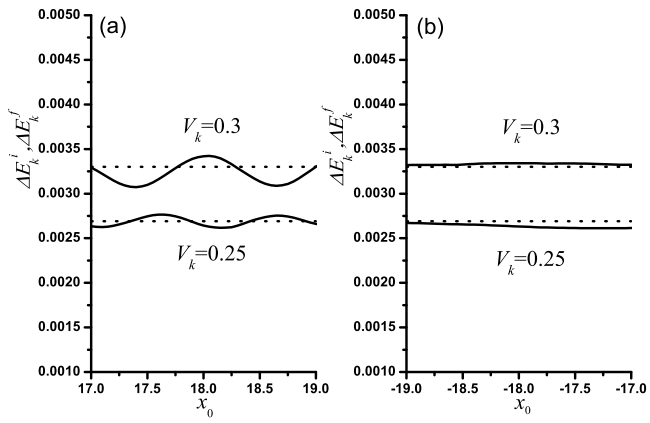

FIG. 4: Numerical results for the continuum model. Amplitude of the kink kinetic energy oscillation before (ΔE_k^i, dotted lines) and after (ΔE_k^f, solid lines) the interaction with the $\mathcal{PT}$-symmetric defect as a function of kink initial position for the two different values of the kink initial velocities, $V_k = 0.25$ and $V_k = 0.3$. The defect amplitude is $\epsilon = 0.15$. In (a) the kink comes from the gain side and (b) from the loss side.

for the continuum system.

B. Kinks with initially excited IM

Here, the scattering of a kink bearing an IM on $\mathcal{PT}$-symmetric defect is considered. The intensity of the IM will be characterized by the amplitude of the kink kinetic energy oscillation caused by the IM, $\Delta E_k = (E_{k,\max} - E_{k,\min})/2$, where $E_{k,\max}$ and $E_{k,\min}$ are the maximum and minimum of the kink kinetic energy.

The kink with the IM is excited with the help of Eq. (5) using the IM amplitude $A = 0.05$ and two values of initial kink velocity, $V_k = 0.25$ and $V_k = 0.3$. For these two cases the amplitude of the initial kink kinetic energy oscillation, ΔE_k^i, is equal to 0.00269 and 0.00330, respectively. These initial values are plotted in Fig. 4 with horizontal dotted lines. Now we calculate the value of ΔE_k^f after the kink passes through the defect with the amplitude $\epsilon = 0.15$ as a function of the kink initial position and present the results by solid lines in Fig. 4 for the kink moving from (a) the gain and (b) the loss side of the defect. In (a), it is clear that the kink's IM is affected by the defect because ΔE_k^f differs from ΔE_k^i, while in (b) they almost coincide, which means that the IM amplitude is not changed by the defect. The oscillation of ΔE_k^f as the function of kink initial position x_0 in (a) has the period close to $V_k(2\pi/\omega)$, which is the distance the kink travels in one period of IM oscillation.

Similar results obtained in frame of the two degree of freedom collective variable model Eqs. (7,8) are presented in Fig. 5. The initial (A_k^i) and final (A_k^f) amplitudes of the kink's shape mode are shown as functions of the kink initial position by the dotted and solid lines, respectively. In (a) the kink hits the defect with amplitude $\epsilon = 0.15$ from the gain side and in (b) from the loss side. The kink initially has IM with the amplitude $A = 0.05$ and the initial velocities of the kinks are $V_k = 0.25$ (thin line) and $V_k = 0.3$ (thick line) in both cases. In very good qualitative agreement with the results for continuum model, the collective variable model shows that in (a) the kink's IM is affected by the defect, while in (b) it is not, since all the three lines overlap.

The results shown in Fig. 6 demonstrate that the kink bearing an excited IM penetrates more easily through the dissipative media. In Fig. 6 (a), the kink critical velocity as a function of the perturbation strength ϵ is shown for the kink bearing an IM with the amplitude $A = 0$ (solid line), $A = 0.05$ (dot-dashed line), and $A = 0.1$ (dot-dot-dashed line). One can see that V_c is almost linear function of ϵ with a slope denoted by σ. It is clear that for given perturbation strength ϵ the critical velocity decreases with increase in the IM amplitude A. In Fig. 6 (b) we plot the value of σ/σ_0 as a function of A, where σ_0 corresponds to $A = 0$. The slope σ decreases with an increasing IM amplitude indicating that the translational degree of freedom of the kink when the IM is excited is less affected by the perturbation. That is to say, the transparency of the defect to the kink transmission is increased as the IM excitation is increased.

In Fig. 7 we contrast the dynamics of the kinks with and without IM in the case of homogeneous perturbation $\gamma(x) \equiv 1$ with (a) $\epsilon = 0.005$ (purely gain, hence acceleration) and (b) $\epsilon = -0.005$ (purely loss, hence deceleration). Two values of initial kink velocities are considered in both cases, namely, 0.15 and 0.3. The kink center

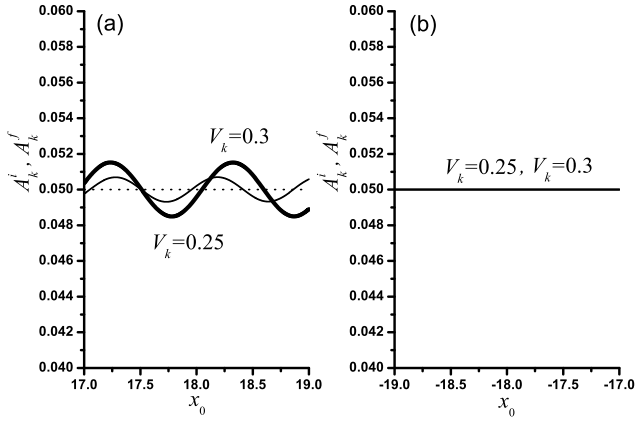

FIG. 5: Collective variable results for the model Eqs. (7,8). The amplitude of the kink's internal shape mode before (A_k^i, dotted lines) and after (A_k^f, solid lines) the interaction with the $\mathcal{PT}$-symmetric defect as a function of the kink initial position for the two different values of the kink initial velocities, $V_k = 0.25$ (thin line) and $V_k = 0.3$ (thick line). The defect amplitude is $\epsilon = 0.15$. In (a) the kink comes from the gain side and (b) from the loss side.

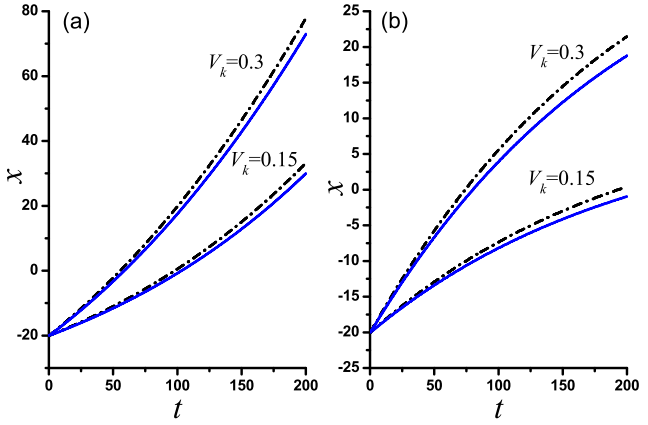

FIG. 7: (Color online) Results for the continuum model. Dynamics of kinks with initial velocities equal to 0.15 and 0.3 in the case of homogeneous perturbation $\gamma(x) \equiv 1$ with (a) $\epsilon = 0.005$ (gain) and (b) $\epsilon = -0.005$ (loss). Solid lines are for the IM amplitude $A = 0$ and dash-dot lines for $A = 0.05$. The kink trajectories show that the velocity of the kink gradually increases in (a) (decreases in (b)), and the kink velocity is always higher for the kink with IM.

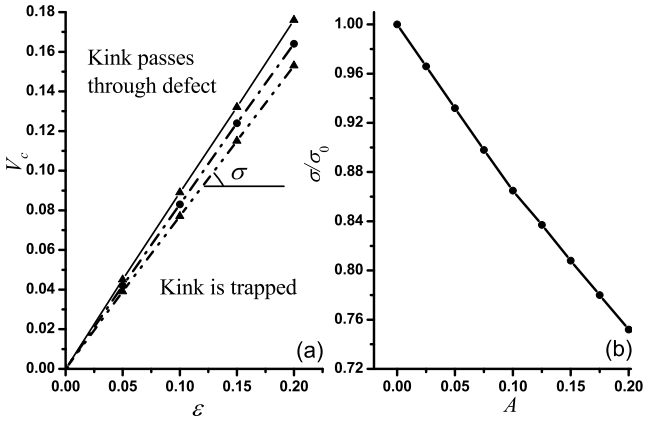

FIG. 6: Results for the continuum model. (a) Relation between the critical initial velocity of the kink and the defect amplitude for the kink with IM amplitude $A = 0$ (solid line), $A = 0.05$ (dot-dash line), and $A = 0.1$ (dot-dot-dash line). The dependencies are nearly linear with the slope σ decreasing with an increase in the IM amplitude A. (b) The value σ/σ_0 as the function of A, where σ_0 corresponds to $A = 0$.

position as a function of time is shown for the cases of no IM, $A = 0$ (solid lines), and for the IM of amplitude $A = 0.05$ (dash-dotted lines). It can be seen that in all cases the kink with an excited IM travels faster than the kink without IM. In other words, the kink bearing IM in the gain media is accelerated faster and in the loss media it is decelerated slower. From here it immediately follows that the phase shift due to interaction with the $\mathcal{PT}$-symmetric defect must be higher (lower) for the kink with IM when it comes from the gain (loss) side. This is illustrated by Fig. 8 in which the kink's phase shift due to interaction with the $\mathcal{PT}$-symmetric defect of strength $\epsilon = 0.2$ is presented as a function of its initial velocity. Solid lines show the results of the numerical solution for the kink without IM, dot-dashed lines indicate the kink bearing an IM with amplitude $A = 0.01$. Note that in (a) the kink moves toward the defect from the gain side and the phase shift is higher for the kink bearing IM. In (b) the kink approaches the defect from the opposite side and the phase shift is higher for the kink without IM. The vertical dotted line in (b) shows the critical value of the initial kink velocity, V_c. For comparison, dashed lines in Fig. 8 show the results obtained with the help of the collective variable method of Eqs. (14) and (16). Note that the accuracy of the collective variable method is very high for the kink without IM.

V. CONCLUSIONS

Interaction of the ϕ^4 kinks with and without IM excitation with the $\mathcal{PT}$-symmetric defect having balanced regions of positive and negative dissipation was investigated numerically, as well as analytically with the help of the collective variable model.

Similar to the SG kink studied earlier [57], a ϕ^4 kink coming from the gain side always passes through the defect and practically restores its initial velocity (see Fig. 1 (a)). For the kink approaching the defect from the opposite side, there exist two different scenarios, depending on the kink initial velocity V_k. For $V_k < V_c$, where V_c is a threshold value of the velocity, the kink does not have enough energy to pass through the defect and it is

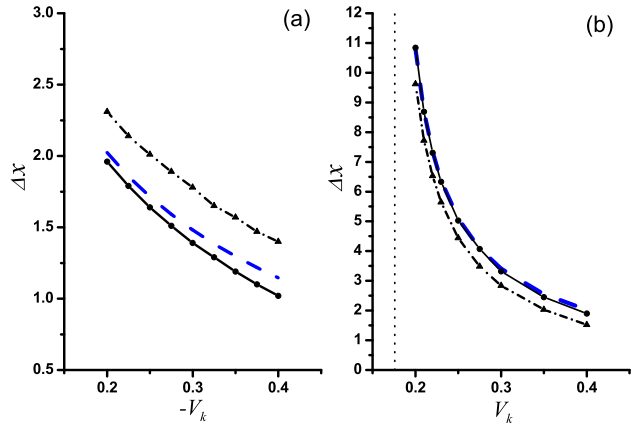

FIG. 8: (Color online) Results for the continuum model and collective variable results of Eqs. (14,16). The kink's phase shift due to the interaction with the $\mathcal{PT}$-symmetric defect as a function of kink initial velocity for the kink moving toward the defect with strength $\epsilon = 0.2$ (a) from the gain side and (b) from the loss side. Solid lines show the results of numerical solution for the kink without IM, dot-dash lines for the kink bearing IM with amplitude $A = 0.01$. Dashed lines show the results obtained with the help of the collective variable method. The vertical dotted line in (b) shows the threshold kink velocity $V_c = 0.176$.

trapped by the lossy side of the defect (see Fig. 1 (b)), while for $V_k > V_c$ it enters the gain region and effectively restores initial velocity.

In contrast to the SG kink, the ϕ^4 kink possesses an internal mode. From our numerical results presented in Fig. 2 it follows that a noticeable IM is excited on the ϕ^4 kink after passing the defect from the gain side and the excitation of IM is much weaker for the kink moving in the opposite direction. The excitation of the kink's IM increases with increasing kink initial velocity; see Fig. 2 (a) and (b). These effects are well reproduced by the two degree of freedom collective variable model Eqs. (7,8), as shown in Fig. 3.

On the other hand, a kink moving from the gain side with an initially excited IM passes through the defect with the IM having, generally speaking, different amplitude, and the effect is stronger for faster kinks [see Fig. 4 (a)]. For the kink moving in the opposite direction the initially excited IM is not affected by the defect [see Fig. 4 (b)]. Analogous results obtained with the use of the collective variable model (see Fig. 5) are in good agreement with the results for the continuum ϕ^4 model shown in Fig. 4.

The kink bearing an IM is faster accelerated in the gain region and slower decelerated in the loss region of the defect in comparison to the kink free of the initially excited IM. As a result, (i) the critical velocity to pass through the loss region is smaller for the kink with IM (see Fig. 6) and (ii) the phase shift due to the passage through the defect increases when the kink with IM hits the defect from the gain side and decreases in the opposite case [see Fig. 8 (a) and (b)].

The single degree of freedom collective variable model gives a very good prediction of the dynamics of the kink's center. Analytical expressions for the kink phase shift and kink critical velocity were derived in frame of this model.

We conclude that the $\mathcal{PT}$-symmetric defects give new opportunities in the manipulation of the soliton dynamics and the presence of the internal modes can induce noticeable asymmetries of the solitary wave-defect interaction both in terms of their excitation, as well as of the kink transmission in the presence of such a mode.

In future work, it would be of interest to study the ϕ^4 kink dynamics in the case of $\mathcal{PT}$-symmetric, periodic $\gamma(x)$. According to the results presented here, kink acceleration can be expected when an IM is excited, even though the gain and loss is balanced in the model. Consideration of the fields with radial symmetry [68] and models of higher dimension is also very tempting. In the one dimensional realm, however, it would also be of particular interest to explore the very rich setting of kink-antikink collisions in the presence of defects. Finally, while a detailed understanding is at this point available based on collective coordinate techniques in the Klein-Gordon field theoretic setting, the picture of soliton-defect interaction and the role of internal modes is far less clear in nonlinear Schrödinger equation settings, where such questions are just starting to be explored [69]. Hence, it would be of particular value to expand on such studies in the near future. These topics are presently under investigation and will be reported in future publications.

Acknowledgments

D.S. thanks the hospitality of the Bashkir State Pedagogical University and acknowledges the financial support from the Institute for Metals Superplasticity Problems, Ufa, Russia. S.V.D. thanks financial support provided by the Russian Government Program 5-100-2020. D.I.B. was partially supported by a grant of Russian Foundation for Basic Research, the grant of the President of Russian Federation for young scientists-doctors of science (project no. MD-183.2014.1) and by the fellowship of Dynasty foundation for young Russian mathematicians. P.G.K. acknowledges support from the US National Science Foundation under grants CMMI-1000337, DMS-1312856, from the ERC and FP7-People under grant IRSES-606096 from the Binational (US-Israel) Science Foundation through grant 2010239, and from the US-AFOSR under grant FA9550-12-10332.

VI. APPENDIX

An attempt to apply commercial symbolic derivation software did not generically provide a satisfactory result. For this reason, in Sec. VI A we calculate analytically the kink critical velocity to pass through the lossy part of the defect and the kink phase shift due to the interaction with the defect. In Sec. VI B, for the particular case of $\beta = \delta_k$, the phase shift is given in a closed form.

A. Analytic results

Given any two numbers $\mathcal{X}_0$ and $\mathcal{X}$, we denote

$$\begin{aligned} g(\mathcal{X}_0,\mathcal{X}) &:= \int\limits_{-\infty}^{+\infty} dx \int\limits_{\mathcal{X}_0}^{\mathcal{X}} \frac{\gamma(x)ds}{\cosh^4(\delta_k(x-s))} \\ &= \int\limits_{-\infty}^{+\infty} dx\,\gamma(x) \int\limits_{\mathcal{X}_0}^{\mathcal{X}} \frac{ds}{\cosh^4\delta_k(x-s)}. \end{aligned} \tag{22}$$

It is clear that for our choice of $\gamma(x)$

$$\gamma(x) = -\frac{1}{\beta}\frac{d}{dx}\frac{1}{\cosh\beta x} \tag{23}$$

and thus we can integrate by parts in (22):

$$\begin{aligned} g(\mathcal{X}_0,\mathcal{X}) = \frac{1}{\beta}\int\limits_{-\infty}^{+\infty} \frac{1}{\cosh\beta x}\left(\frac{1}{\cosh^4(\delta_k(x-\mathcal{X}))}\right. \\ \left. -\frac{1}{\cosh^4\delta_k(x-\mathcal{X}_0)}\right)dx. \end{aligned}$$

We introduce the notation

$$G(\mathcal{X}) := \frac{1}{\beta}\int\limits_{-\infty}^{+\infty} \frac{dx}{\cosh\beta x\cosh^4\delta_k(x-\mathcal{X})} \tag{24}$$

and see that

$$g(\mathcal{X}_0,\mathcal{X}) = G(\mathcal{X}) - G(\mathcal{X}_0). \tag{25}$$

By a simple change of variable $x \mapsto \delta_k x$ we reduce the formula for $G(\mathcal{X})$ to

$$G(\mathcal{X}) = \frac{1}{\beta\delta_k}\int\limits_{-\infty}^{+\infty} \frac{dx}{\cosh\frac{\beta}{\delta_k}x\cosh^4(x-\delta_k\mathcal{X})}. \tag{26}$$

Now we make our main assumption:

$$\beta = \frac{2m-1}{n}\delta_k, \quad n,m\in\mathbb{N}. \tag{27}$$

This assumption is quite general in the sense that given any β and δ_k, we can always approximate with any prescribed accuracy the fraction β/δ_k choosing appropriate m and n.

In view of (27) formula (26) casts into the form

$$G(\mathcal{X}) = \frac{n}{(2m-1)\delta_k^2}\int\limits_{-\infty}^{+\infty} \frac{dx}{\cosh\frac{2m-1}{n}x\cosh^4(x-\delta_k\mathcal{X})}.$$

Here we make one more change of variable $x = n\ln y$. It yields

$$G(\mathcal{X}) = \frac{2^5n^2}{(2m-1)\delta_k^2}\mathrm{e}^{4\delta_k\mathcal{X}}G_1(\mathrm{e}^{2\delta_k\mathcal{X}}), \tag{28}$$

where

$$\begin{aligned} G_1(\mathcal{Y}) &:= \int\limits_0^{+\infty} \frac{y^{4n+2m-2}dy}{(y^{4m-2}+1)(y^{2n}+\mathcal{Y})^4} \\ &= \frac{1}{2}\int\limits_{-\infty}^{+\infty} \frac{y^{4n+2m-2}dy}{(y^{4m-2}+1)(y^{2n}+\mathcal{Y})^4}, \quad \mathcal{Y}>0. \end{aligned}$$

It is straightforward to check that

$$\begin{aligned} G_1(\mathcal{Y}) &= \frac{1}{12}\frac{d^2G_2}{d\mathcal{Y}^2}(\mathcal{Y}), \\ G_2(\mathcal{Y}) &:= \int\limits_{-\infty}^{+\infty} \frac{y^{4n+2m-2}dy}{(y^{4m-2}+1)(y^{2n}+\mathcal{Y})^2}. \end{aligned} \tag{29}$$

The differentiation w.r.t. a parameter $\mathcal{Y}$ is possible, since the integral in the definition of $G_2(\mathcal{Y})$ converges uniformly in $\mathcal{Y}$. We also observe that although formally it is possible, we do not pass to the third derivative w.r.t. $\mathcal{Y}$ in the latter formula since it leads us to a diverging integral.

We calculate function G_2 by means of complex analysis. Namely, we employ an approach based on finding residues, see for instance, [70, Ch. VI, Sect. 3]. In accordance with these approach, we first regard y as a complex variable and consider the integrand in (29) as a meromorphic function defined on the complex plane $\mathbb{C}$. Then in accordance with the Cauchy theorem function G_2 is given by the formula:

$$G_2(\mathcal{Y}) = 2\pi\mathrm{i}\sum_j \operatorname*{res}_{y=y_j} \frac{y^{4n+2m-2}}{(y^{4m-2}+1)(y^{2n}+\mathcal{Y})^2}, \tag{30}$$

where i stands for the imaginary unit and the sum is taken over all the poles in the complex upper half-plane $\operatorname{Im} y > 0$. The symbol $\operatorname*{res}_{y=y_j} f$ denotes the residue of the function at a pole y_j. We recall that the residue at $y = y_j$ of a meromorphic function is a coefficient at the power $(y-y_j)^{-1}$ in the Laurent expansion for a function at point y_j.

In our case the poles are exactly the roots of the equation

$$(y^{4m-2}+1)(y^{2n}+\mathcal{Y})^2 = 0.$$

The roots located in the complex upper half-plane are

$$y_j^{(m)} = \mathrm{e}^{\frac{\mathrm{i}\pi(2j+1)}{4m-2}}, \quad j = 0, \dots, 2m-2,$$
$$y_j^{(n)} = \mathcal{Y}^{\frac{1}{2n}} \mathrm{e}^{\frac{\mathrm{i}\pi(2j+1)}{2n}}, \quad j = 0, \dots, n-1.$$

To calculate the residues at these poles, we need to find the coefficients $c_j^{(\natural)}$ in the expansions

$$\frac{y^{4n+2m-2}}{(y^{4m-2}+1)(y^{2n}+\mathcal{Y})^2} = \dots + \frac{c_j^{(\natural)}}{y - y_j^{(\natural)}} + \dots, \quad (31)$$

as $y \to y_j^{(\natural)}$, where $\natural = n, m$.

Suppose $\mathcal{Y} \neq 1$ and let us find first the desired coefficients for $y_j^{(m)}$. We should just represent $(y^{4m-2}+1)$ as

$$y^{4m-2} + 1 = (y - y_j^{(m)}) P_j^{(m)}(y), \quad (32)$$

where $P_j^{(m)}$ is a some polynomial. Then

$$c_j^{(m)} = \frac{(y_j^{(m)})^{4n+2m-2}}{P_j^{(m)}(y_j^{(m)}) \left((y_j^{(m)})^{2n} + \mathcal{Y}\right)^2}.$$

Differentiating (30) w.r.t. y and letting then $y = y_j^{(m)}$, we get

$$P_j^{(m)}(y_j^{(m)}) = (4m-2)(y_j^{(m)})^{4m-3} = -\frac{4m-2}{y_j^{(m)}}. \quad (33)$$

Hence,

$$\begin{aligned} c_j^{(m)} =& -\frac{(y_j^{(m)})^{2m+4n-1}}{(4m-2)\left((y_j^{(m)})^{2n} + \mathcal{Y}\right)^2} \\ =& \frac{(y_j^{(m)})^{4n-1}}{(4m-2)\left((y_j^{(m)})^{2n} + \mathcal{Y}\right)^2} \\ =& \frac{\mathrm{e}^{\frac{\mathrm{i}\pi}{4m-2}(2j+1)(4n-1)}}{(4m-2)\left(\mathrm{e}^{\frac{\mathrm{i}\pi n}{2m-1}(2j+1)} + \mathcal{Y}\right)^2}, \end{aligned} \quad (34)$$

where $j = 0, \dots, 2m-2$.

The calculations of the residues for $y_j^{(n)}$ are more tricky since the function in the right hand side of (29) has second order poles at $y_j^{(n)}$. By analogy with (32) we introduce the representation

$$y^{2n} + \mathcal{Y} = (y - y_j^{(n)}) P_j^{(n)}(y) \quad (35)$$

and differentiating it once and twice and letting then $y = y_j^{(n)}$, in the same way as in (33) we obtain

$$\begin{aligned} P_j^{(n)}(y_j^{(n)}) &= -\frac{2n\mathcal{Y}}{y_j^{(n)}}, \\ \frac{dP_j^{(n)}}{dy}(y_j^{(n)}) &= -\frac{n(2n-1)\mathcal{Y}}{(y_j^{(n)})^2}. \end{aligned} \quad (36)$$

Let $h(y) := y^{4n+2m-2}/(y^{4m-2}+1)$, then it follows from (31) that

$$\begin{aligned} c_j^{(n)} =& \frac{d}{dy}\frac{h}{(P_j^{(n)})^2}\bigg|_{y=y_j^{(n)}} \\ =& \frac{h'(y_j^n)}{\left(P_j^{(n)}(y_j^n)\right)^2} - \frac{2h(y_j^{(n)})P_j^{(n)\prime}(y_j^{(n)})}{\left(P_j^{(n)}(y_j^{(n)})\right)^3}. \end{aligned}$$

Thus, due to the definition of h, $y_j^{(n)}$, and (36)

$$\begin{aligned} c_j^{(n)} =& \frac{h'(y_j^n)(y_j^{(n)})^2 - (2n-1)h(y_j^{(n)})y_j^{(n)}}{4n^2\mathcal{Y}^2} \\ =& \frac{h(y_j^{(n)})y_j^{(n)}}{4n^2\mathcal{Y}^2}\left(y_j^{(n)}\frac{d\ln h}{dy}(y_j^n) - 2n + 1\right) \\ =& \frac{1}{4n^2}\left(2n + 2m - 1 + \frac{4m-2}{(y_j^{(n)})^{4m-2}+1}\right) \\ & \cdot \frac{(y_j^{(n)})^{2m-1}}{(y_j^{(n)})^{4m-2}+1} \\ =& \frac{1}{4n^2}\left(2n - 2m - 1 + \frac{4m-2}{\mathcal{Y}^{\frac{2m-1}{n}}\mathrm{e}^{\frac{\mathrm{i}\pi(2j+1)(2m-1)}{2n}}+1}\right) \\ & \cdot \frac{\mathcal{Y}^{\frac{2m-1}{2n}}\mathrm{e}^{\frac{\mathrm{i}\pi(2j+1)(2m-1)}{2n}}}{\mathcal{Y}^{\frac{2m-1}{n}}\mathrm{e}^{\frac{\mathrm{i}\pi(2j+1)(2m-1)}{n}}+1}. \end{aligned}$$

We substitute the above formulae and (34) for the residues into (30) and obtain the final expression for G_2:

$$\begin{aligned} G_2(\mathcal{Y}) =& \frac{\pi\mathrm{i}}{2m-1}\sum_{j=0}^{2m-2}\frac{\mathrm{e}^{\frac{\mathrm{i}\pi(2j+1)(4n-1)}{4m-2}}}{\left(\mathrm{e}^{\frac{\mathrm{i}\pi n}{4m-2}(2j+1)} + \mathcal{Y}\right)^2} \\ &+ \frac{\pi\mathrm{i}}{2n^2}\sum_{j=0}^{n-1}\left(2n - 2m - 1 + \frac{4m-2}{\mathcal{Y}^{\frac{2m-1}{n}}\mathrm{e}^{\frac{\mathrm{i}\pi(2j+1)(2m-1)}{2n}}+1}\right) \\ & \cdot \frac{\mathcal{Y}^{\frac{2m-1}{2n}}\mathrm{e}^{\frac{\mathrm{i}\pi(2j+1)(2m-1)}{2n}}}{\mathcal{Y}^{\frac{2m-1}{n}}\mathrm{e}^{\frac{\mathrm{i}\pi(2j+1)(2m-1)}{n}}+1}. \end{aligned}$$

In view of (29) it leads us to the formula for G_1:

$$\begin{aligned} G_1(\mathcal{Y}) =& \frac{\pi\mathrm{i}}{4m-2}\sum_{j=0}^{2m-2}\frac{\mathrm{e}^{\frac{\mathrm{i}\pi(2j+1)(4n-1)}{4m-2}}}{\left(\mathrm{e}^{\frac{\mathrm{i}\pi n}{2m-1}(2j+1)} + \mathcal{Y}\right)^4} \\ &+ \frac{\pi\mathrm{i}}{24n^2}\sum_{j=0}^{n-1}\frac{d^2}{d\mathcal{Y}^2}\left(2n - 2m - 1 + \frac{4m-2}{\mathcal{Y}^{\frac{2m-1}{n}}\mathrm{e}^{\frac{\mathrm{i}\pi(2j+1)(2m-1)}{2n}}+1}\right) \\ & \cdot \frac{\mathcal{Y}^{\frac{2m-1}{2n}}\mathrm{e}^{\frac{\mathrm{i}\pi(2j+1)(2m-1)}{2n}}}{\mathcal{Y}^{\frac{2m-1}{n}}\mathrm{e}^{\frac{\mathrm{i}\pi(2j+1)(2m-1)}{n}}+1}. \end{aligned} \quad (37)$$

Although in the above calculations we have supposed that $\mathcal{Y} \neq 1$, it is clear that G_1 is a continuous function and thus we can find $G_1(1)$ as

$$G_1(1) = \lim_{\mathcal{Y}\to 1} G_1(\mathcal{Y}).$$

It also follows from (25), (28) that the critical velocity is given by the formula

$$\begin{aligned} V_c =& \frac{\epsilon\delta_k^2}{M} g(0,\mathcal{X}_0) \\ =& \frac{32n^2\epsilon\delta_k^2}{M(2m-1)}\left(G_1(1) - \mathrm{e}^{4\delta_k\mathcal{X}_0} G_1(\mathrm{e}^{2\delta_k\mathcal{X}_0})\right), \end{aligned} \tag{38}$$

where G_1 is determined by the above formulae.

In particular, if $n = m = 1$, then $\beta = \delta_k$,

$$\begin{aligned} G_1(\mathcal{Y}) &= \frac{\pi}{32}\frac{\mathcal{Y}^3 - 9\mathcal{Y}^2 + 16\mathcal{Y}^{\frac{3}{2}} - 9\mathcal{Y} + 1}{\mathcal{Y}^{\frac{3}{2}}(\mathcal{Y}-1)^4} \\ &= \frac{\pi}{32}\frac{\mathcal{Y} + 4\mathcal{Y}^{\frac{1}{2}} + 1}{\mathcal{Y}^{\frac{3}{2}}(\mathcal{Y}^{\frac{1}{2}}+1)^4}, \\ G_1(1) &= \frac{3\pi}{256}. \end{aligned} \tag{39}$$

For $n = 2$, $m = 1$ we have $\beta = \delta_k/2$,

$$\begin{aligned} &G_1(\mathcal{Y}) = \frac{\pi}{512\mathcal{Y}^{\frac{7}{4}}(1+\mathcal{Y})^4}\big(5\sqrt{2}\mathcal{Y}^{\frac{7}{2}} - 7\sqrt{2}\mathcal{Y}^3 + 35\sqrt{2}\mathcal{Y}^{\frac{5}{2}} \\ &- 105\sqrt{2}\mathcal{Y}^2 - 105\sqrt{2}\mathcal{Y}^{\frac{3}{2}} + 256\mathcal{Y}^{\frac{7}{4}} + 35\sqrt{2}\mathcal{Y} \\ &- 7\sqrt{2}\mathcal{Y}^{\frac{1}{2}} + 5\sqrt{2}\big), \\ &G_1(1) = \frac{256 - 144\sqrt{2}}{8192}\pi. \end{aligned} \tag{40}$$

B. Phase shift

We find the phase shift only in the case $\beta = \delta_k$, i.e., for $n = m = 1$ in (27). The reason is that in other cases the calculations become too bulky and yield finally multiline formulae. One more reason is that for other values of m and n, in the calculations we face with the problem of finding roots for polynomials of high degrees and we can not find them explicitly.

We proceed to the calculations. First we compare formulae (15) and (22) and see that by (25)

$$F(z) - B = -\frac{1}{\delta_k} g(z, +\infty) = \frac{1}{\delta_k} G(z).$$

Hence, it follows from (28), (39) that

$$F(z) - B = \frac{2^5}{\delta_k^3}\mathrm{e}^{4\delta_k z} G_1(\mathrm{e}^{2\delta_k z}) = \frac{\pi}{\delta_k^3}\frac{\mathrm{e}^{\delta_k z}(\mathrm{e}^{2\delta_k z} + 4\mathrm{e}^{\delta_k z} + 1)}{(\mathrm{e}^{\delta_k z}+1)^4}.$$

We substitute this formula into (14) and make the change of variable $y = \mathrm{e}^{\delta_k Z}$:

$$\Delta x = \pm\frac{1}{\delta_k} G_3\left(-\frac{MV_k\delta_k^4}{\pi\epsilon}\right), \tag{41}$$

$$G_3(\mathcal{Z}) := \int_0^{+\infty} \frac{(y^2+4y+1)dy}{y(y^2+4y+1) - \mathcal{Z}(y+1)^4}. \tag{42}$$

It is easy to check the estimate

$$0 \leqslant \frac{y(y^2+4y+1)}{(y+1)^4} \leqslant \frac{3}{8}, \quad y \in [0, +\infty),$$

and thus, function $G_3(\mathcal{Z})$ is well-defined only for $\mathcal{Z} \in (-\infty, 0) \cup (3/8, +\infty)$. In what follows we assume that $\mathcal{Z} = -\frac{MV_k\delta_k^4}{\pi\epsilon}$ ranges exactly in this domain.

The integrand in (42) is a rational function and to integrate it, we need to expand it into the sum of simple fractions. The latter requires the knowledge of the roots for the denominator. Fortunately, we are able find these roots explicitly. They are given by the identities:

$$\begin{aligned} y_1 :=& -\frac{4\mathcal{Z} - 1 + \sqrt{1+8\mathcal{Z}}}{4\mathcal{Z}} \\ &+ \frac{\sqrt{1 + (4\mathcal{Z}-1)\sqrt{1+8\mathcal{Z}}}}{2\sqrt{2}\mathcal{Z}}, \\ y_2 :=& -\frac{4\mathcal{Z} - 1 + \sqrt{1+8\mathcal{Z}}}{4\mathcal{Z}} \\ &- \frac{\sqrt{1 + (4\mathcal{Z}-1)\sqrt{1+8\mathcal{Z}}}}{2\sqrt{2}\mathcal{Z}}, \\ y_3 :=& -\frac{4\mathcal{Z} - 1 - \sqrt{1+8\mathcal{Z}}}{4\mathcal{Z}} \\ &+ \frac{\sqrt{1 - (4\mathcal{Z}-1)\sqrt{1+8\mathcal{Z}}}}{2\sqrt{2}\mathcal{Z}}, \\ y_4 :=& -\frac{4\mathcal{Z} - 1 - \sqrt{1+8\mathcal{Z}}}{4\mathcal{Z}} \\ &- \frac{\sqrt{1 - (4\mathcal{Z}-1)\sqrt{1+8\mathcal{Z}}}}{2\sqrt{2}\mathcal{Z}}. \end{aligned} \tag{43}$$

Generally speaking, there roots are complex-valued and this is why we fix the branch of the square root by the requirement $\sqrt{\mathrm{e}^{\mathrm{i}\theta}} = \mathrm{e}^{\mathrm{i}\frac{\theta}{2}}$, $\theta \in (-\pi, \pi]$.

We consider first the case $1 + 8\mathcal{Z} < 0$, i.e., $\mathcal{Z} \in (-\infty, -1/8)$. Here all the roots are complex-valued. Roots y_1 and y_3 are complex-conjugate and the same is true for y_2, y_4:

$$\begin{aligned} y_1 = P_1 + \mathrm{i}Q_1, \quad y_2 = P_2 + \mathrm{i}Q_2, \\ y_3 = P_1 - \mathrm{i}Q_1, \quad y_4 = P_2 - \mathrm{i}Q_2. \end{aligned} \tag{44}$$

The denominator in (42) obeys the representation:

$$\begin{aligned} &y(y^2+4y+1) - \mathcal{Z}(y+1)^4 \\ &\qquad = -\mathcal{Z}\big((y-P_1)^2 + Q_1^2\big)\big((y-P_2)^2 + Q_2^2\big). \end{aligned}$$

By means of this representation it is straightforward to make sure that

$$\begin{aligned} \frac{(y^2+4y+1)dy}{y(y^2+4y+1) - \mathcal{Z}(y+1)^4} =& -\frac{1}{\mathcal{Z}}\left(\frac{K_1(y-P_1) + K_2}{(y-P_1)^2 + Q_1^2}\right. \\ &\left. - \frac{K_1(y-P_2) + K_3}{(y-P_2)^2 + Q_2^2}\right), \end{aligned}$$

where

$$\begin{aligned}
K_1 :=&\frac{K_3-K_2+1}{P_1-P_2},\\
K_2 :=&\Big(\big((Q_2^2+Q_1^2+(P_2-P_1)^2\big)(P_1^2+4P_1+1)\\
&+Q_1^2\big(P_1^2+Q_1^2-P_2^2-Q_2^2-2P_1P_2-8P_2-2\big)\Big)\\
&/\Big((P_2^2+Q_2^2-P_1^2-Q_1^2)^2\\
&-4(P_1-P_2)(P_2(P_1^2+Q_1^2)-P_1(P_2^2+Q_2^2))\Big),\\
K_3 :=&-\Big(\big((Q_2^2+Q_1^2+(P_2-P_1)^2\big)(P_2^2+4P_2+1)\\
&+Q_2^2\big(P_2^2+Q_2^2-P_1^2-Q_1^2-2P_1P_2-8P_1-2\big)\Big)\\
&/\Big((P_2^2+Q_2^2-P_1^2-Q_1^2)^2\\
&-4(P_1-P_2)(P_2(P_1^2+Q_1^2)-P_1(P_2^2+Q_2^2))\Big).
\end{aligned}\tag{45}$$

Now we employ obvious formulae

$$\begin{aligned}
&\int\left(\frac{K_1(y-P_1)+K_2}{(y-P_1)^2+Q_1^2}-\frac{K_1(y-P_2)+K_3}{(y-P_2)^2+Q_2^2}\right)dy\\
&=\frac{K_1}{2}\ln\frac{(y-P_1)^2+Q_1^2}{(y-P_2)^2+Q_2^2}\\
&\quad+\frac{K_2}{Q_1}\arctan\frac{y-P_1}{Q_1}-\frac{K_3}{Q_2}\arctan\frac{y-P_2}{Q_2}
\end{aligned}$$

to obtain

$$\begin{aligned}
G_3(\mathcal{Z}) =&\frac{K_1}{2\mathcal{Z}}\ln\frac{P_1^2+Q_1^2}{P_2^2+Q_2^2}-\frac{\pi}{2\mathcal{Z}}\left(\frac{K_2}{|Q_1|}-\frac{K_3}{|Q_2|}\right)\\
&-\frac{K_2}{Q_1\mathcal{Z}}\arctan\frac{P_1}{Q_1}+\frac{K_3}{Q_2\mathcal{Z}}\arctan\frac{P_2}{Q_2}.
\end{aligned}$$

This formula, (45), (43), (44), (42), and (41) provide the final expression for the phase shift once $\frac{MV_k\delta_k^4}{\pi\epsilon}>\frac{1}{8}$.

We proceed to the case $\mathcal{Z}\in(-1/8,0)$. Here all the roots $y_1,\dots,y_4$ are real and negative. The denominator in (42) can be represented as

$$y(y^2+4y+1)-\mathcal{Z}(y+1)^4=-\mathcal{Z}(y-y_1)(y-y_2)(y-y_3)(y-y_4).$$

The integrand in (42) can be expanded as

$$\begin{aligned}
\frac{y^2+4y+1}{y(y^2+4y+1)-\mathcal{Z}(y+1)^4}=-\frac{1}{\mathcal{Z}}\Bigg(&\frac{R_1}{y-y_1}+\frac{R_2}{y-y_2}\\
&+\frac{R_3}{y-y_3}+\frac{R_4}{y-y_4}\Bigg),
\end{aligned}$$

where

$$\begin{aligned}
R_1 :=&\frac{y_1^2+4y_1+1}{(y_1-y_2)(y_1-y_3)(y_1-y4)},\\
R_2 :=&\frac{y_2^2+4y_2+1}{(y_2-y_1)(y_2-y_3)(y_2-y4)},\\
R_3 :=&\frac{y_3^2+4y_3+1}{(y_3-y_1)(y_3-y_2)(y_3-y4)},\\
R_4 :=&\frac{y_4^2+4y_4+1}{(y_4-y_1)(y_4-y_2)(y_4-y3)}.
\end{aligned}\tag{46}$$

Integrating the obtained identity, we get

$$G_3(\mathcal{Z})=\frac{1}{\mathcal{Z}}\sum_{j=1}^{4}R_j\ln|y_j|.\tag{47}$$

Together with (41), (42), (43), (46) it leads us to the formula for the phase shift as $0<\frac{MV_k\delta_k^4}{\pi\epsilon}<\frac{1}{8}$.

It remains to study the case $\mathcal{Z}\in(3/8,+\infty)$. Here the roots y_1, y_2 are real and negative, while y_3, y_4 are complex-valued and complex conjugate:

$$y_3=P_3+\mathrm{i}Q_3,\quad y_4=P_3-\mathrm{i}Q_3.\tag{48}$$

The representation for the denominator in (42) reads as

$$y(y^2+4y+1)-\mathcal{Z}(y+1)^4=-\mathcal{Z}(y-y_1)(y-y_2)\big((y-P_3)^2+Q_3^2\big).$$

The integrand in (42) satisfies the identity

$$\begin{aligned}
\frac{y^2+4y+1}{y(y^2+4y+1)-\mathcal{Z}(y+1)^4}=-\frac{1}{\mathcal{Z}}\Bigg(&\frac{L_1}{y-y_1}+\frac{L_2}{y-y_2}\\
&-\frac{(L_1+L_2)(y-P_3)+L_3}{(y-P_3)^2+Q_3^2}\Bigg),
\end{aligned}$$

where

$$\begin{aligned}
L_1 :=&\frac{y_1^2+4y_1+1}{\big((P_3-y_1)^2+Q_3^2\big)(y_1-y_2)},\\
L_2 :=&\frac{y_2^2+4y_2+1}{\big((P_3-y_2)^2+Q_3^2\big)(y_2-y_1)},\\
L_3 :=&-P_3(L_1+L_2)+y_1L_1+y_2L_2-1.
\end{aligned}\tag{49}$$

Integrating the above formulae, we arrive at

$$\begin{aligned}
G_3(\mathcal{Z})=\frac{1}{\mathcal{Z}}\Bigg(&L_1\ln|y_1|+L_2\ln|y_2|\\
&-\frac{L_1+L_2}{2}\ln(P_3^2+Q_3^2)\\
&+\frac{\pi L_3}{2|Q_3|}+\frac{L_3}{Q_3}\arctan\frac{P_3}{Q_3}\Bigg).
\end{aligned}$$

This formula, (41), (42), (43), (48), (49) yield the analytic expression for the phase shift once $\frac{MV_k\delta_k^4}{\pi\epsilon}<-\frac{3}{8}$.

[1] C. M. Bender and S. Boettcher, Phys. Rev. Lett. **80**, 5243 (1998).
[2] C. M. Bender, D. C. Brody, and H. F. Jones, Phys. Rev. Lett. **89**, 270401 (2002).
[3] C. E. Ruter, K. G. Markris, R. El-Ganainy, D. N. Cristodoulides, M. Segev, and D. Kip, Nat. Phys. **6**, 192 (2010).
[4] A. Guo, G. J. Salamo, D. Duchesne, R. Morandotti, M. Volatier-Ravat, V. Aimez, G. A. Siviloglou, and D. N. Christodoulides, Phys. Rev. Lett. **103**, 093902 (2009).
[5] A. Regensburger, C. Bersch, M. A. Miri, G. Onishchukov, D. N. Christodoulides, and U. Peschel, Nature (London) **488**, 167 (2012).
[6] A. Regensburger, M. A. Miri, C. Bersch, J. Nager, G. Onishchukov, D. N. Christodoulides, and U. Peschel, Phys. Rev. Lett. **110**, 223902 (2013).
[7] B. Peng, S. K. Ozdemir, F. Lei, F. Monifi, M. Gianfreda, G. L. Long, S. Fan, F. Nori, C. M. Bender, and L. Yang, Nat. Phys. **10**, 394 (2014).
[8] B. Peng, S. K. Ozdemir, S, Rotter, H. Yilmaz, M. Liertzer, F. Monifi, C. M. Bender, F. Nori, L. Yang, Science **346**, 328-332 (2014).
[9] J. Schindler, A. Li, M. C. Zheng, F. M. Ellis, and T. Kottos, Phys. Rev. A **84**, 040101 (2011).
[10] J. Schindler, Z. Lin, J. M. Lee, H. Ramezani, F. M. Ellis, and T. Kottos, J. Phys. A: Math. Theor. **45**, 444029 (2012).
[11] N. Bender, S. Factor, J. D. Bodyfelt, H. Ramezani, D. N. Christodoulides, F. M. Ellis, and T. Kottos, Phys. Rev. Lett. **110**, 234101 (2013).
[12] C. M. Bender, B. Berntson, D. Parker, and E. Samuel, Am. J. Phys. **81**, 173 (2013).
[13] M. C. Zheng, D. N. Christodoulides, R. Fleischmann, and T. Kottos, Phys. Rev. A **82**, 010103 (2010).
[14] S. Longhi, Phys. Rev. A **81**, 022102 (2010).
[15] H. Cartarius and G. Wunner, Phys. Rev. A **86**, 013612 (2012); J. Phys. A: Math. Theor. **45**, 444008 (2012).
[16] E.-M. Graefe, J. Phys. A: Math. Theor. **45**, 444015 (2012).
[17] A. S. Rodrigues, K. Li, V. Achilleos, P. G. Kevrekidis, D. J. Frantzeskakis, and C. M. Bender, Rom. Rep. Phys. **65**, 5 (2013).
[18] V. Achilleos, P. G. Kevrekidis, D. J. Frantzeskakis, and R. Carretero-González Phys. Rev. A **86**, 013808 (2012).
[19] H. Ramezani, T. Kottos, V. Kovanis, and D. N. Christodoulides, Phys. Rev. A **85**, 013818 (2012).
[20] A. E. Miroshnichenko, B. A. Malomed, and Yu. S. Kivshar, Phys. Rev. A **84**, 012123 (2011).
[21] C. T. West, T. Kottos, and T. Prosen, Phys. Rev. Lett. **104**, 054102 (2010).
[22] A. A. Sukhorukov, S. V. Dmitriev, S. V. Suchkov, and Yu. S. Kivshar, Opt. Lett. **37**, 2148 (2012).
[23] F. Nazari, M. Nazari, and M. K. Moravvej-Farshi, Opt. Lett. **36**, 4368 (2011).
[24] J. D'Ambroise, P. G. Kevrekidis and S. Lepri, J. Phys. A: Math. Theor. **45**, 444012 (2012).
[25] J. D'Ambroise, S. Lepri, B. A. Malomed, P.G. Kevrekidis, arXiv:1407.1086, Phys. Lett. A (in press).
[26] I. V. Barashenkov, S. V. Suchkov, A. A. Sukhorukov, S. V. Dmitriev, and Yu. S. Kivshar, Phys. Rev. A 86, 053809 (2012).
[27] S. V. Suchkov, S. V. Dmitriev, A. A. Sukhorukov, I. V. Barashenkov, E. R. Andriyanova, K. M. Badgetdinova, and Yu. S. Kivshar, Appl. Phys. A - Mater. **115**, 443 (2014).
[28] L. Kh. Rysaeva, S. V. Suchkov, and S. V. Dmitriev, JETP Lett., **99**, 577 (2014).
[29] S. V. Dmitriev, S. V. Suchkov, A. A. Sukhorukov, and Yu. S. Kivshar, Phys. Rev. A **84**, 013833 (2011).
[30] S. V. Suchkov, S. V. Dmitriev, B. A. Malomed, and Yu. S. Kivshar, Phys. Rev. A 85, 033825 (2012).
[31] S. V. Suchkov, A. A. Sukhorukov, S. V. Dmitriev, and Yu. S. Kivshar, Europhys. Lett., **100**, 54003 (2012).
[32] K. Li and P. G. Kevrekidis Phys. Rev. E **83**, 066608 (2011).
[33] I. V. Barashenkov, G. S. Jackson, and S. Flach, Phys. Rev. A **88**, 053817 (2013).
[34] J. Pickton and H. Susanto, Phys. Rev. A **88**, 063840 (2013).
[35] P. G. Kevrekidis, D. E. Pelinovsky, and D. Y. Tyugin, SIAM J. Appl. Dyn. Sys. SIAM J. Appl. Dyn. Sys. **12**, 1210 (2013).
[36] P. G. Kevrekidis, D. E. Pelinovsky, and D. Y. Tyugin, J. Phys. A: Math. Theor. **46**, 365201 (2013).
[37] D. E. Pelinovsky, D. A. Zezyulin, and V. V. Konotop, J. Phys. A: Math. Theor. **47**, 085204 (2014).
[38] K. Li, P. G. Kevrekidis, B. A. Malomed, and U. Günther, J. Phys. A: Math. Theor. **44**, 444021 (2012).
[39] S. V. Dmitriev, A. A. Sukhorukov, and Yu. S. Kivshar, Opt. Lett. **35**, 2976 (2010).
[40] N. V. Alexeeva, I. V. Barashenkov, K. Rayanov and S. Flach, Phys. Rev. A **89**, 013848 (2014).
[41] H. Xu, P. G. Kevrekidis, A. Saxena, arXiv:1404.4382.
[42] I. V. Barashenkov, Phys. Rev. A **90**, 045802 (2014).
[43] P. G. Kevrekidis, Phys. Rev. A **89**, 010102 (2014).
[44] A. Demirkaya, D. J. Frantzeskakis, P. G. Kevrekidis, A. Saxena, and A. Stefanov, Phys. Rev. E **88**, 023203 (2013).
[45] A. Demirkaya, T. Kapitula, P. G. Kevrekidis, M. Stanislavova, and A. Stefanov, Stud. Appl. Math. **133**, 298 (2014).
[46] N. Lu, P. G. Kevrekidis, and J. Cuevas-Maraver, J. Phys. A: Math. Theor. **47**, 455101 (2014).
[47] S. V. Dmitriev and P. G. Kevrekidis, Soliton Collisions, in The Sine-Gordon Model and Its Applications, edited by J. Cuevas- Maraver, P. G. Kevrekidis, and F. Williams (Springer, Cham, 2014), pp. 5995.
[48] S. V. Dmitriev, Yu. S. Kivshar, and T. Shigenari, Phys. Rev. E **64**, 056613 (2001).
[49] S. V. Dmitriev, P. G. Kevrekidis, and Yu. S. Kivshar, Phys. Rev. E **78**, 046604 (2008).
[50] A. E. Miroshnichenko, S. V. Dmitriev, A. A. Vasiliev, and T. Shigenari, Nonlinearity **13**, 837 (2000).
[51] Yu. S. Kivshar and B. A. Malomed, Phys. Lett. A **129**, 443 (1988).
[52] Yu. S. Kivshar, B. A. Malomed, and A. A. Nepomnyashchy, Sov. Phys. JETP **67**(4), 850 (1988).
[53] B. A. Malomed, J. Phys. A **25**, 755 (1992).
[54] Z. Fei, Yu. S. Kivshar, and L. Vazquez, Phys. Rev. A **45**, 6019, (1992).

[55] Z. Fei, Yu. S. Kivshar, and L. Vazquez, Phys. Rev. A **46**, 5214, (1992).
[56] B. Piette and W. J. Zakrzewski, Phys. Rev. E. **79**, 046603 (2009).
[57] D. Saadatmand, S. V. Dmitriev, D. I. Borisov, and P. G. Kevrekidis, Phys. Rev. E, **90**, 052902 (2014).
[58] Yu. S. Kivshar, D. E. Pelinovsky, T. Cretegny, and M. Peyrard, Phys. Rev. Lett. **80**, 5032 (1998).
[59] N. R. Quintero and P. G. Kevrekidis, Phys. D **170**, 31 (2002).
[60] D. K. Campbell, J. S. Schonfeld, and C. A. Wingate, Phys. D **9**, 1 (1983).
[61] T. I. Belova and A. E. Kudryavtsev, Phys. Usp. **40**, 359 (1997).
[62] R. H. Goodman and R. Haberman, SIAM J. Appl. Dyn. Sys. **4**, 1195 (2005).
[63] Yu. S. Kivshar, Z. Fei, and L. Vazquez, Phys. Rev. Lett. **67**, 1177 (1991).
[64] B. A. Malomed, Phys. D **15**, 385 (1985).
[65] I. V. Barashenkov and O. F. Oxtoby, Phys. Rev. E **80**, 026608 (2009).
[66] O. M. Braun and Yu. S. Kivshar, *The Frenkel-Kontorova Model: Concepts, Methods, and Applications* (Springer, Berlin, 2004).
[67] Yu. S. Kivshar and B. A. Malomed, Rev. Mod. Phys. **61**, 763 (1989).
[68] J. G. Caputo and M. P. Soerensen, Phys. Rev. E **88**, 022915 (2013).
[69] N. Karjanto, W. Hanif, B. A. Malomed and H. Susanto, arXiv:1401.4241.
[70] M. A. Evgrafov, *Analytic functions* (Nauka, Moscow, 1991) (in Russian).